Experimental investigation of the atmospheric boundary layer flow past a building model with openings

Marinos Manolesos[1,2,a], Zhiqiu Gao[1], Demetri Bouris[3]

[1]State Key Laboratory of Atmospheric Boundary Layer Physics and Atmospheric Chemistry, Institute of Atmospheric Physics, Chinese Academy of Sciences
Beijing 100029, China

[2]School of Engineering, Swansea University, Bay Campus, Fabian Way, Swansea, SA1 8EN, UK

[3]Laboratory for Innovative Environmental Technologies, School of Mechanical Engineering, National Technical University of Athens, 9 Iroon Polytechneiou str., 15780 Athens, Greece.

Abstract

As modern building design moves towards more sustainable solutions the use of natural ventilation is one of the options considered to improve indoor air quality and to minimize the energy cost of the buildings. The present cross-ventilation study is an experimental investigation of the atmospheric boundary layer flow past a cubic building model with vertical openings. Wind tunnel experiments were performed for two different simulated upstream boundary layer conditions and for two different cube options (with and without openings). Pressure measurements on the building model surface are in very good agreement with benchmark measurements. Stereo Particle Image Velocimetry measurements were performed to examine the effect of both the upstream condition and the openings. It is found that both conditions significantly alter the pressure and flow structure around the building model. Ventilation rate is estimated using two methods, the orifice equation and the measured velocity profile in the vicinity of the apertures. The comparison shows that the orifice equation overpredicts the ventilation rate and the effect of the upstream boundary layer. All data in the present report are freely available for validation purposes.

1 Introduction

Knowledge of the details of the flow field in and around buildings and of the pressure distribution on their external surfaces provides crucial information for numerous applications. These include those related to occupant comfort, the operation, structural integrity and energy performance of the buildings themselves (natural ventilation, wind loads, infiltration, heat losses etc.) and those related to energy systems that depend on the building geometry (urban wind turbines, solar collectors etc.). When it comes to sustainable or zero energy buildings and healthy environments, natural ventilation is a crucial factor [1, 2]. It is an integral part of modern building design and it is usually combined with active ventilation features in hybrid systems in order to achieve higher energy efficiency [3].

[a]Author to whom all correspondence should be addressed. Email: marinos.manolesos@swansea.ac.uk, Tel. +44 1792 295514

Wind induced ventilation and more specifically cross-ventilation is both pressure and momentum driven [4, 5] so, for an effective design, the performance of different building components and the interaction among and with the wind environment should be known accurately. Numerous studies have dealt with the issue of ventilation performance assessment and recent reviews have been provided by different authors [6-9].

Wind tunnel tests can be used for natural ventilation design [10], or for CFD validation purposes [11-14], which is a requirement from the numerical point of view [15]. In the latter exercise, also known as *validation application* [16, 17], experimental results are considered benchmark cases for Computational Fluid Dynamic (CFD) simulations [5, 18-22] or analytical descriptions [23-26]. Although the comparison of experimental results with mathematical model predictions seems like a straightforward task, it should be performed with great care and vigilance from both sides (numerical and experimental) in order to avoid systematic errors. As highlighted in the past, caution should be exercised to avoid comparing *apples with oranges* [27]. On the other hand, a fruitful application of the cross-comparison between wind tunnel measurements and CFD simulations can lead the development of best practice guidelines for CFD applications [28-30].

Among the wind engineering experimental investigations, the effect of the upstream boundary layer (BL) characteristics, such as ground shear velocity and Turbulence Intensity (TI), on the structure of the flow past buildings has been a subject of previous research [31-33]. However, to the authors' knowledge, there is a scarcity of experimental studies that include scaled atmospheric BL simulations in the study of the flow past buildings with a porous envelope, with reference to natural ventilation applications.

One of the limiting factors of relevant flow field experimental campaigns up to now was that they provided point measurements [34], with very limited use of non-intrusive field methods, such as Particle Image Velocimetry (PIV) [11] and practically no use of Stereo PIV [35]. In addition, all ventilation studies concerned horizontal, square or round openings, that did not necessarily scale with the upstream BL and/or the building itself and therefore their vertical positioning had little relevance to the natural ventilation application [11, 14, 36].

The additional challenge in the latter case is that the pressure distribution along the opening is not constant and hence the orifice equation cannot be used for airflow rate prediction. The orifice equation is widely used in cross-ventilation studies, despite the fact that it has been known to give questionable predictions even for simple aperture geometries [12, 37]. In general, natural ventilation flow rate prediction is considered a particularly challenging task and even more sophisticated methods can have a significant error margin. In fact, significant discrepancies between the flow rate measured at the windward and the leeward opening have been reported [38-40].

The present study is a wind tunnel investigation of wind driven cross-ventilation. The aim is to provide further insight into the interaction of basic cross-ventilation flow characteristics in and around the building and, additionally, to generate an experimental data base that may be used to validate CFD codes. The building model is a cube with vertically distributed openings and a clearly defined interior geometry. The cube is embedded in a controlled simulated atmospheric BL. Pressure and Stereo PIV measurements are presented in order to examine the effect of upstream conditions on cross-ventilation and the effect of the latter on the flow around the building.

It is noted that a generic cubic building shape has been chosen and that the vertical openings are not intended to simulate a scaled version of a single opening on the building face. At the achieved scale of 1:400 (see section 2.3), the dependence of the opening's discharge coefficient on the opening Reynolds number would not permit scale similarity [1]. The vertical openings were chosen in order to study their effect on and interaction with the simulated upstream atmospheric boundary layer and the building surface pressure distribution. While there have been studies that investigated the effect of the relative position of single openings on cross ventilation [9, 11, 20], experimental investigations of vertical openings along the full height of the building remain limited [41-43].

It has been well documented from early on in the literature [31-33] that the surface pressure distribution depends on the upstream boundary layer characteristics but also that, except close to the edges, the pressure coefficient is nearly constant along any horizontal level on a windward or leeward face, varying mostly in the vertical direction. Considering a single opening at the centre of each horizontal level on the windward and leeward face and integrating the openings of all horizontal levels leads to the vertical openings of the form being applied here. This allows for a simple and easily modelled configuration that provides the opportunity for insight regarding the interdependence of the vertical distribution of the upstream flow and the building surface pressure distribution with the flow's penetration of the building envelope.

The novelty of the study lies in the common scaling of the building, openings and varying upstream BL profiles, the orientation of the openings and the provision of detailed 3D experimental measurements of the mean and turbulent characteristics of the flow around the building. It is aspired that the present contribution, dealing with a case that has seldom been studied in the past, will provide not only insight but also high accuracy detailed experimental data suitable for validation purposes. The present paper aims at presenting the findings of the study, while, for validation purposes, all data are freely available online [44] to the interested researcher.

2 Methods

2.1 Wind tunnel and cube model

All experiments were performed at the National Technical University of Athens, in the large test section (3.5m x 2.5m x 12.0m – width x height x length) of the low speed wind tunnel. The latter is a closed-circuit facility with a maximum speed of 15m/s at the specific test section. A schematic view of the complete set up is given in Figure 1, and an upstream view is given in Figure 2.

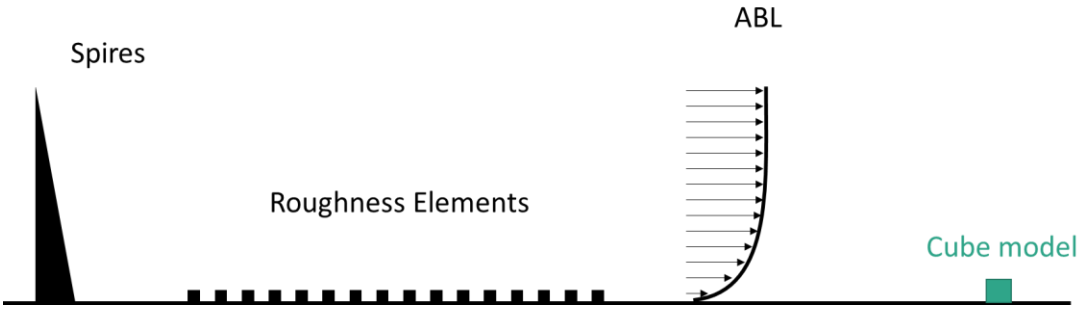

Figure 1. Schematic side view of the experimental set up. The Spires and roughness elements used to create the atmospheric boundary layer (ABL) are shown along with the cube model.

Figure 2. View of the test section, looking upstream. The spires, and roughness elements are visible with the Plexiglas model located at the centre of the turntable.

A plexiglass cube with an edge length of 110mm, located at the centre of the wind tunnel turntable was used as the building model. The cube had vertical slot openings of 90x6 mm^2 on each vertical side that acted as the openings for the cross-ventilation study, giving a maximum porosity of 4.5%. The openings could be fully open or covered, depending on the desired opening orientation and distribution. A CAD model and a photograph of the cube are shown in Figure 3, while the pressure tap positions are given in Figure 4.

One of the cube side faces was fitted with a 6x7 grid of pressure taps, while the cube top face had a grid of 7x7 taps. The taps had an internal diameter of 0.6mm and were connected to a pressure scanner via silicone tubes. Pressure measurements on all sides of the cube were performed by rotating the cube to the desired position each time.

The sidewall tubes were concealed inside the cube “hollow walls” to avoid interference with the internal flow. The tubes corresponding to the cube roof passed through a rectangular hollow column located at the centre of the tube. The column location was dictated by space requirements for the tubing and, since pressure distributions on all sides of the building were obtained by rotating the model, the central position of the column ensured symmetry. Furthermore, it acted as a well-defined obstacle to the direct cross-flow when windward and leeward apertures were open. This set-up is shown schematically in Figure 5.

The column spanned the full internal height of the cube and had square cross-section with a side of 22mm. This resulted in an internal blockage ratio of 22%, for the cross-sections containing the column and 0% everywhere else. It is expected that the blockage effect of the column will be easy to quantify numerically, however, this was not possible with the available experimental data.

The fact that the tubing was in a confined and well-defined space substantially facilitates the numerical mesh generation procedure for this case. This was a priority since one of the main objectives of the study was to create experimental data for the validation numerical codes. Additionally, this made the model more robust, enhancing the repeatability of the measurements.

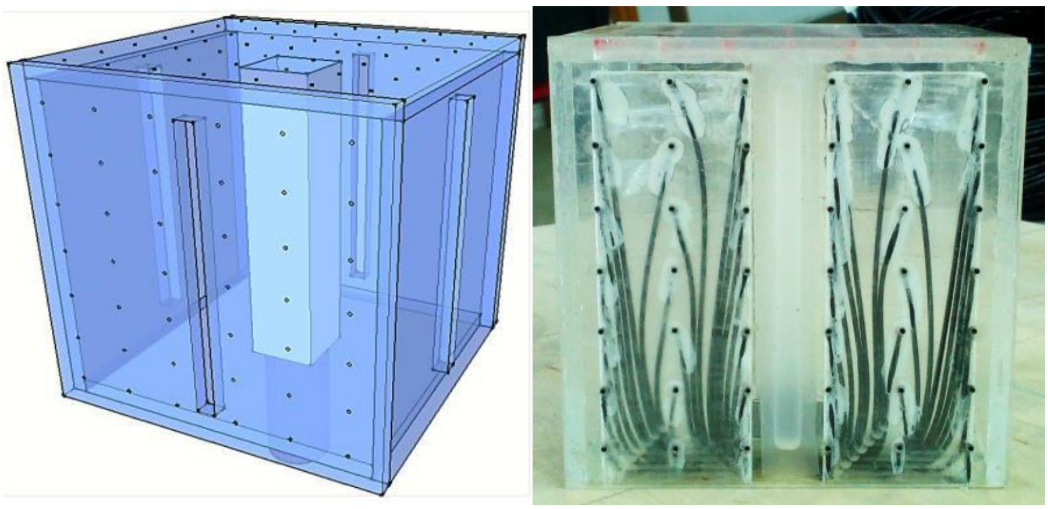

Figure 3. (Left) 3D view of the plexiglass cube with visible slot openings on all sides, pressure tap positions on the roof and a single sidewall and the inner column concealing the pressure tubing and (right) front view of the actual cube model.

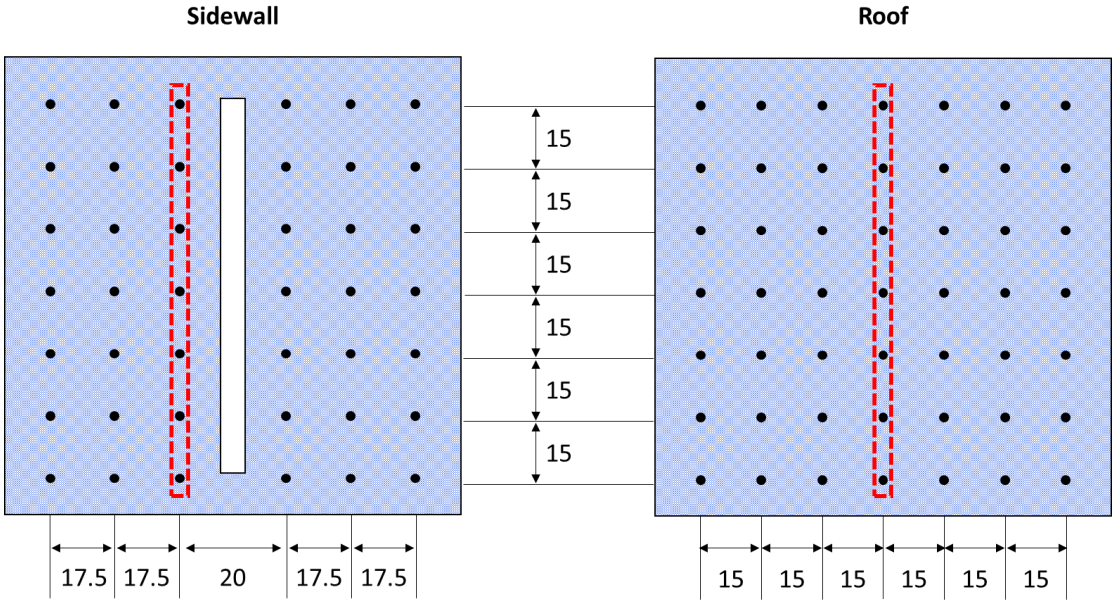

Figure 4. Schematic view of the cube faces with the pressure taps. (Left) Front and rear faces and (right) top face. The red dashed lines enclose the pressure taps used for the centre line pressure plots. Dimensions are given in mm.

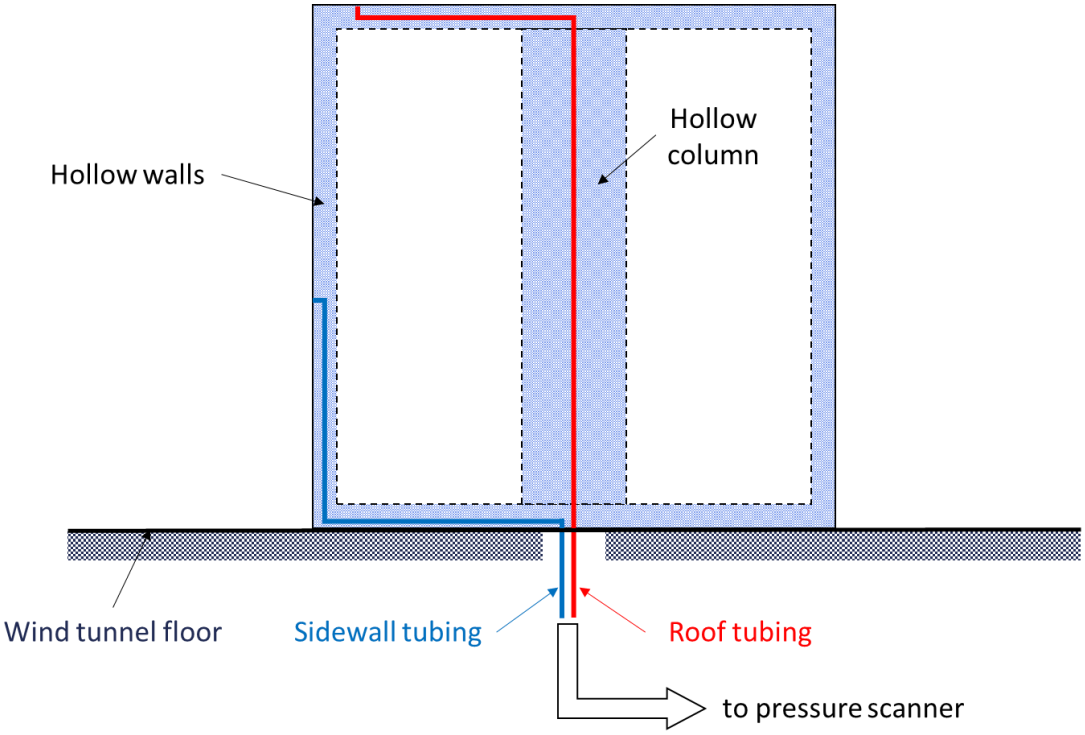

Figure 5: Schematic representation of the cube model with internal tubing for the sidewall and roof taps. The sidewall openings are not shown.

2.2 Measurement set-up

2.2.1 Hot wire and pressure

The generated atmospheric BL was measured using a TSI Inc. IFA 300 measurement system with a single wire probe (TSI 1201), that was calibrated in-situ prior to the measurements. The uncertainty for the hot wire measurements was <2%.

The pressure taps were connected to a pressure scanner (FCS421, Furness Controls Ltd) and through that to a differential manometer (FCO16, Furness Controls Ltd). The sampling rate was 50Hz and only average values are considered in this investigation, as due to the length of the tubes connecting the tap with the pressure scanner, high frequency information was lost. The 95% confidence interval for the pressure measurements was at worst 3%.

2.2.2 Stereo-PIV

For the Stereo-PIV measurements two TSI Powerview Plus™ 4MP Cameras were used that were located inside the test section. The technique described and used in [45, 46] was applied to quantify the effect of camera vibration which was found negligible. The Stereo PIV set up also included a 200mJ Nd:YAG Litron laser and a commercial droplet generator (TSI model 9307) that created olive oil droplets with a mean diameter of 1μm. The cameras were located at the sides of the model and the laser sheet was directed to the desired location by means of a mirror located on the wind tunnel traverse system, well above the cube.

A pulse separation time of 85 μsec was used as higher values would increase the measurement noise and make peak detection harder. The corresponding minimum resolved velocity (i.e. the velocity corresponding to a displacement of 0.1px [47, 48]) was equal to 0.12m/s, which means that any values below this should not be trusted. A discussion on the error sources in PIV can be found in [49, 50].

Image post processing was performed using the TSI Inc software Insight. The number of spurious vectors was always below 5% and they were replaced using a 3 × 3 vector local median. The particle displacement was in all cases less than 1/4 of the 32 × 32px interrogation area and a 50% overlapping was used, which lead to a spacing of 1.8mm between vectors in all dimensions, see also Table 1. For each plane, 1000 snapshots were taken and the averaged data are presented here. Velocity derivatives were computed using the least squares method which is second order accurate, cancels out the effect of oversampling and produces smoother results [51]. All PIV results are scaled with cube height, h, and the velocity above the incoming BL, U_{ref}.

Table 1. Stereo PIV test details for all the planes measured

Final interrogation area size [px]	32
Final interrogation area size [mm]	1.8
Minimum resolvable velocity [m/s]	0.12
Minimum resolvable velocity [normalized with respect to the free stream]	2%
Number of snapshots per plane	1000

In total, four measurement planes are discussed in the present report, three parallel to the flow (A, B and C) and one normal to it (plane D). The parallel planes are along the cube centreline upstream, above and downstream of the cube. Plane D is parallel to the cube front face and at its side. All planes are show in Figure 6 and Figure 7.

Data closer to the cube than 1cm were affected by reflections off the cube surface and are masked out in this report. The camera orientation in Stereo PIV is not normal to the light sheet, which makes the specific issue even more challenging, although similar problems have been reported in simpler 2D PIV configurations [11, 52]. It was possible to minimize the region affected by the reflections during the present campaign to 1cm by locally painting the cube model in a matt black paint and by masking parts of the camera view. Other methods were tried as well, such as the use of Rhodamine 6B and lens filters, but they did not prove beneficial in the present case. Additionally, a background reflection image was subtracted from the raw images prior to processing, in order to enhance image correlation in the affected areas.

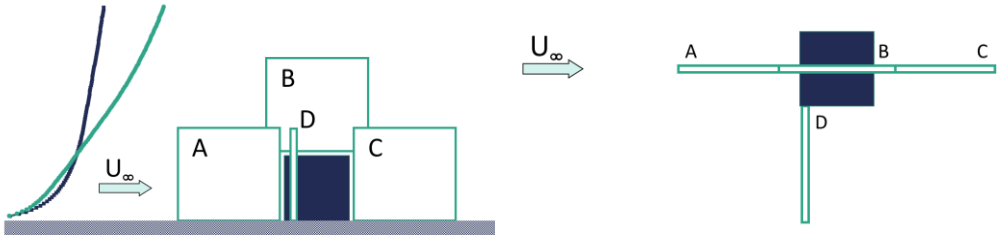

Figure 6. Side (left) and top (right) view of the measurement planes A, B, C and D in green outline. The cube is dark blue and the flow is from left to right. The two different boundary layers examined are also shown schematically.

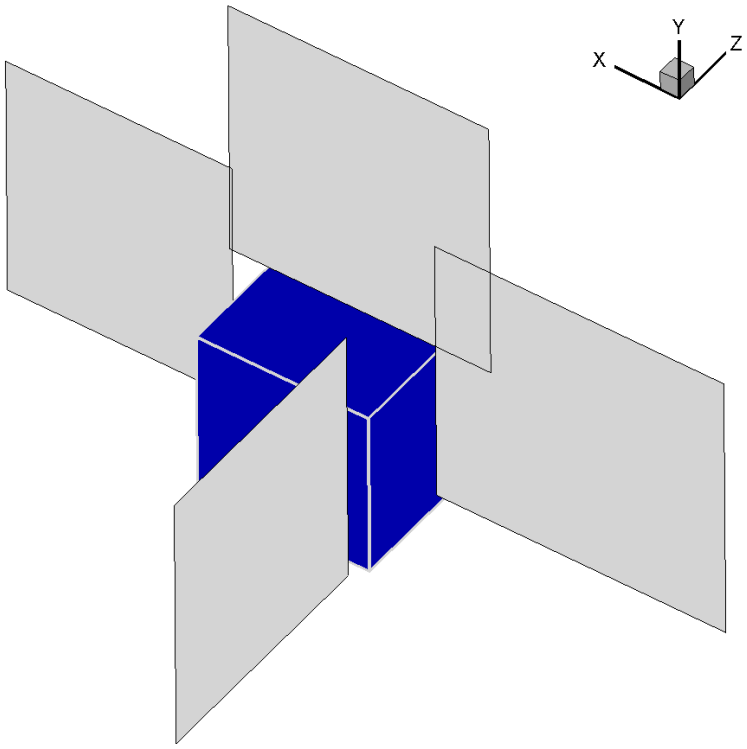

Figure 7. 3D view of the Stereo PIV measurement planes around the cube. The flow is along the x axis, y is the vertical direction and z is the spanwise direction.

2.3 Simulated Atmospheric Boundary Layers

The upstream BL [53, 54] was generated by a combination of spires and roughness elements based on the method of Irwin [55]. Two different conditions were examined, one with High Shear (HS) velocity profile and one with Low Shear (LS), as shown in Figure 8. The HS profile had a TI of 18% at cube height and a power law exponent of α = 0.22, while the LS profile had a TI of 12% and an exponent of α = 0.12. Details of the simulated BL profiles are given in Table 2, while, for completeness, the power law is given in equation (1), where U_h is the velocity at cube height (in its absence), h is the cube height and y is the vertical coordinate.

$$u(y)/U_h = (y/h)^{\alpha} \quad (1)$$

The Reynolds number at cube height was above 2.0e4, i.e. over the suggested limit for Reynolds number independence of the flow [31, 56]. Reynolds number was defined as in equation (2), where ν is the kinematic viscosity.

$$Re_h = U_h * h/\nu \quad (2)$$

The BL profiles were measured using a hot wire probe. Each point was measured twice for 105sec at 10kHz sampling rate. The spectra of the axial turbulence component are given in Figure 9, where it can be seen that a -5/3 inertial subrange slope exists for more than a decade of non-dimensional frequency. Based on the BL mean profile and turbulence characteristics, the model scale factor [57] was 1:400, up to a height of ~0.3m i.e. 3 times

the model height. It is noted that the scale factor can be relaxed by a factor of 2 at least for pressure data, since it yields errors of the order of 10% [58].

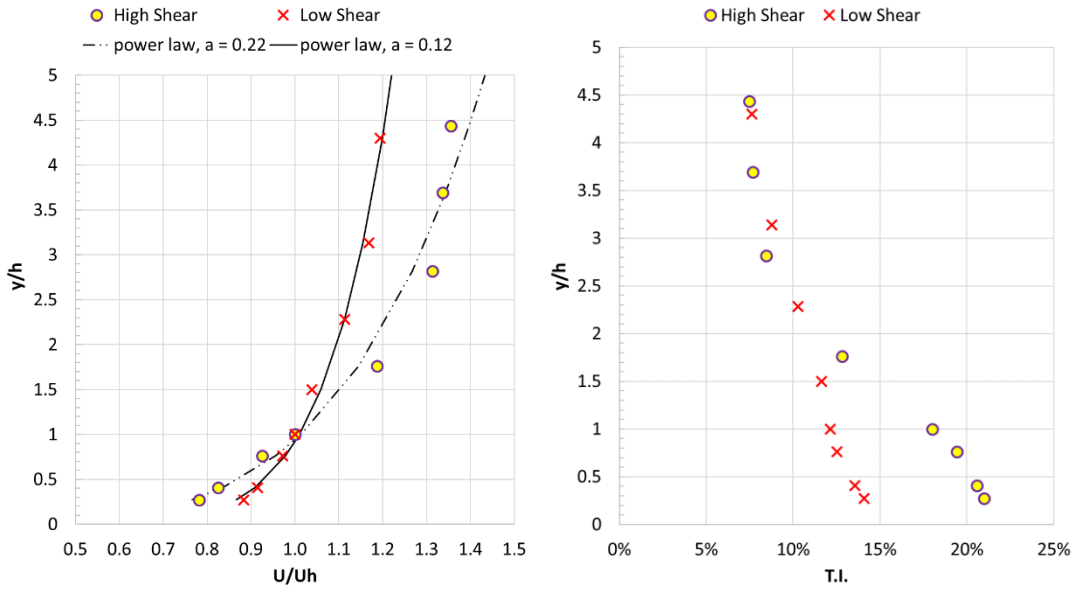

Figure 8. Measured profiles of mean velocity (left) and streamwise turbulence intensity (right) corresponding to the Low and High Shear inflow cases.

Table 2. Details of the approaching turbulent boundary layers

	High Shear	Low Shear
Abbreviation	HS	LS
Power law exponent	0.22	0.12
TI at cube height	18%	12%
Velocity at cube height, U_h [m/s]	3.2	3.5
Velocity above the BL, U_{ref} [m/s]	5.06	5.04
Reynolds number	2.4e4	2.4e4

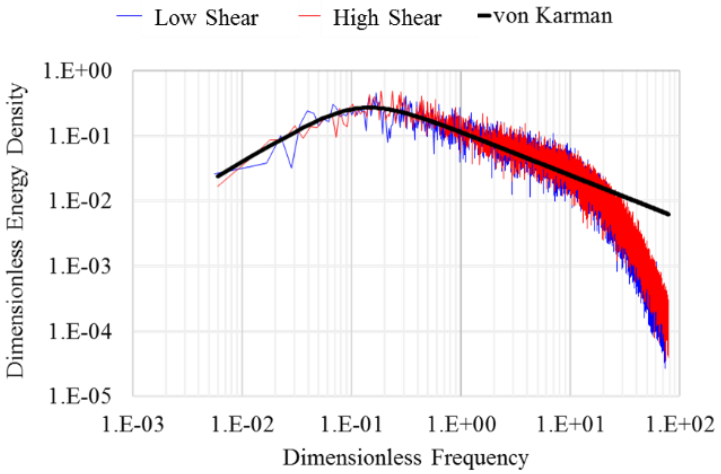

Figure 9. Non-dimensional spectra of the velocity at cube height for both upstream conditions.

2.4 Configurations

Besides the upstream conditions, the only other parameter to be varied during the present investigation was the cube openings (Open or Closed), while the cube orientation was always normal to the free stream.

In the case where the openings were open, the cube slots on the windward and leeward faces of the cube were left open to allow cross-ventilation. For simplicity, the two configurations will be referred to as Closed and Open in the remaining of the text. Accordingly, the two different inflow profiles will be distinguished based on their mean velocity shear characteristic (high or low), although as explained in the previous section more characteristics differ between the two. Table 3 lists the cases examined in this study.

Table 3. The cases examined in the present study

Case	Inflow	Openings	Cube orientation
1	High Shear	Closed	0°
2	High Shear	Open	0°
3	Low Shear	Closed	0°
4	Low Shear	Open	0°

3 Results

3.1 Validation

In [59] twelve institutes participated in a comparative program and performed wind tunnel surface measurements on a cubic model embedded in a turbulent BL with a profile exponent of α = 0.22 ± 0.02, i.e. under conditions similar to the HS profile of the present investigation. The participants were free to perform the tasks according to their judgement and standards and, in total, 15 sets of measurements were provided. Results exhibiting significant deviations were excluded from the reduced sample, the average values of which is considered to be the benchmark for the case.

The mean pressure coefficient, C_p, was calculated based on the velocity at cube height, see equation (3), where P is the pressure on the cube, P_{ref} is the pressure well above the BL, ρ the air density and U_h the velocity at cube height.

$$C_p = \frac{P - P_{ref}}{0.5 * \rho * U_h^2} \tag{3}$$

In Figure 11 the benchmark data from [59], individual results with high deviations (Extreme Cases – EC) from [59] and measurements from the present campaign are presented using the same scaling. The agreement of the present results with the benchmark data is considered very good and well within the range of the original benchmark study [59].

For the present results, at the front and rear cube faces, the taps left of the opening slot are considered, which were 10mm left of the geometrical cube centre line, see also Figure 4. The path on the cube faces is also shown on Figure 10.

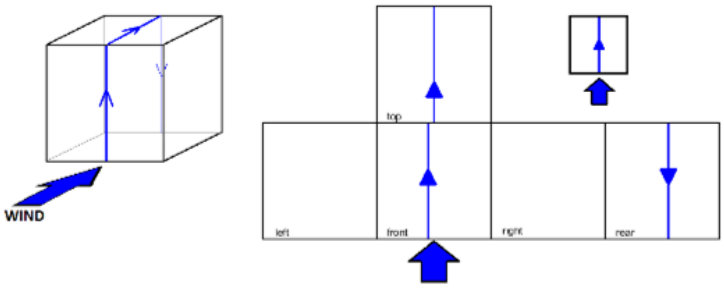

Figure 10. Path along the cube centre line, see also Figure 4 for the specific pressure taps.

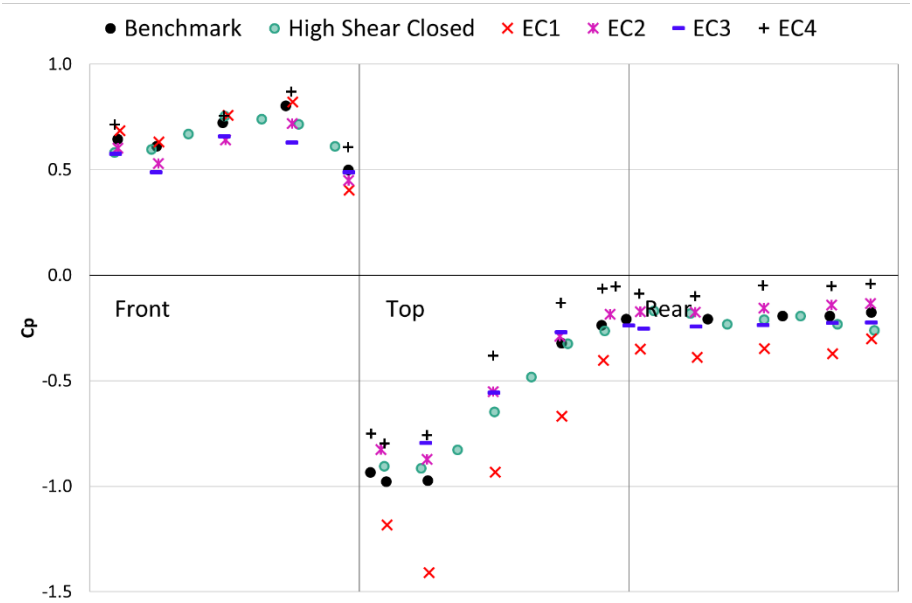

Figure 11. Pressure coefficient distribution along the cube centreline for the Closed High Shear case and comparison with benchmark data and results with the highest deviations (Extreme Cases – EC) from [59].

3.2 Pressure measurements

Figure 12 presents the pressure coefficient distribution along the cube centre line for all four cases. The differences in the oncoming BL shear properties lead to the differences on the windward face pressure coefficient, suggesting that the horseshoe vortex that forms upstream of the cube is different. The effect is more pronounced for the Closed cases but is also evident for the Open cases. The effect of the openings is not as pronounced on the windward face.

The main differences are observed on the top face. The HS cases have a significantly lower suction peak close to the cube edge and a sharper pressure drop indicating a shorter reattachment length. As on the front face, the effect of the openings is less pronounced than that of the oncoming flow.

Smaller discrepancies are observed on the leeward side, where the base pressure level is slightly lower for the LS than for the HS cases. Also, the Open cases have lower pressure level than the Closed cases.

Overall the pressure measurements suggest that the flow structure is different between the LS and the HS cases, especially over the top face and in the wake of the building model. As discussed in the following section, Stereo PIV velocity measurements confirm this finding.

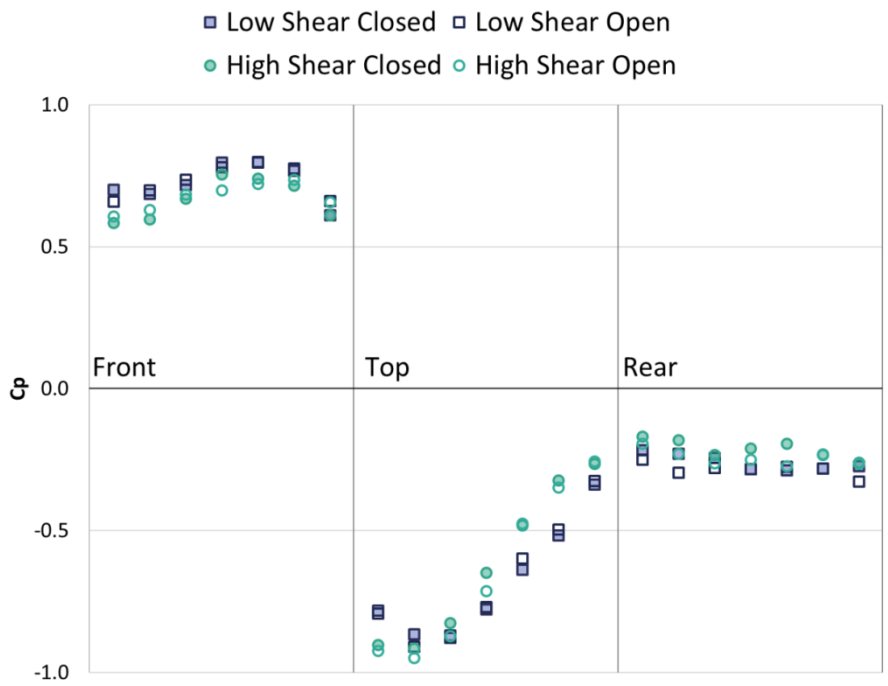

Figure 12. Pressure coefficient distribution along the cube centreline for all the cases considered in this study.

3.3 Stereo PIV results

3.3.1 Planes parallel to the flow

Figure 13 presents streamwise velocity contours on the planes along the cube centreline (planes A, B and C) for all the examined cases. The oncoming BL is also shown schematically. All data are non-dimensionalized with the undisturbed velocity above the BL, U_{ref}, unless otherwise stated.

The velocity measurements confirm the indications of the pressure data presented in the previous section, as, indeed, the flow structure between the LS and the HS cases is different. In the LS results the roof recirculation region is larger and extends higher and further downstream than in the HS cases, as highlighted by the red arrow in Figure 13. Additionally, in the wake of the HS cases, a saddle point is observed on the plane downstream of the building model. The flow structure upstream and above the cube remains unchanged regardless of the state of the cube slots (Open or Closed) .

In all cases the streamlines downstream of a cube form a vortex core, which is the trace of the arch-type vortex that forms downstream of the tube [60]. The centre of the vortex, as defined by the streamlines, is affected by the upstream condition (it moves downstream for the HS case) and the openings (moves downstream and lower for the Open cases), as shown in Figure 14.

Shear ($\overline{u'v'}$, Figure 15) and normal (Figure 16 to Figure 18) Reynolds stress contours are discussed next. In all cases, two regions of high Reynolds stress values are observed, one above and downstream of the top recirculation region and the other above and downstream of the arch-type vortex. The Reynolds stress concentration is higher for the LS cases, which suggests a stronger flapping of the shear layer above the reversed flow regions (above the roof and above the arch type vortex). The Closed cases also have higher Reynolds stress values and at larger areas than the Open cases, which indicates that the outflow from the opening reduces the unsteadiness of the flow in the wake of the cube.

In the Open cases, regions of high $\overline{u'u'}$ also appear downstream of the opening, indicating variation of the flow in the streamwise direction and more so for the LS case. On the contrary, $\overline{v'v'}$ and $\overline{w'w'}$ in the same area appear relatively small, suggesting there is a well-directed outflow in the region.

Due to reflections from the WT floor it was possible to capture only the upper part of the horseshoe vortex (see also Figure 13). Its unsteady nature and movement leads to increased values of $\overline{u'u'}$ (Figure 16) and $\overline{v'v'}$ (Figure 17) upstream of the cube and results suggest that the vortex moves closer to the cube for the Open cases.

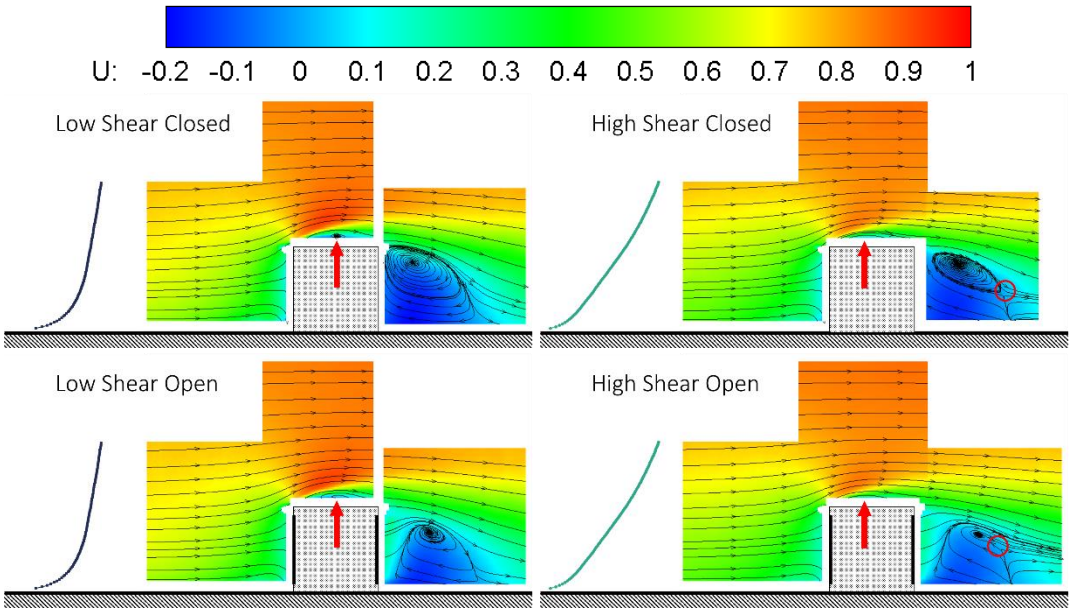

Figure 13. Streamwise velocity contours and in-plane flow lines on the planes along the cube centreline (A, B and C) for all cases. Saddle point location indicated by a red circle. The red arrows indicate the location of peak curvature of the streamlines over the cube top face.

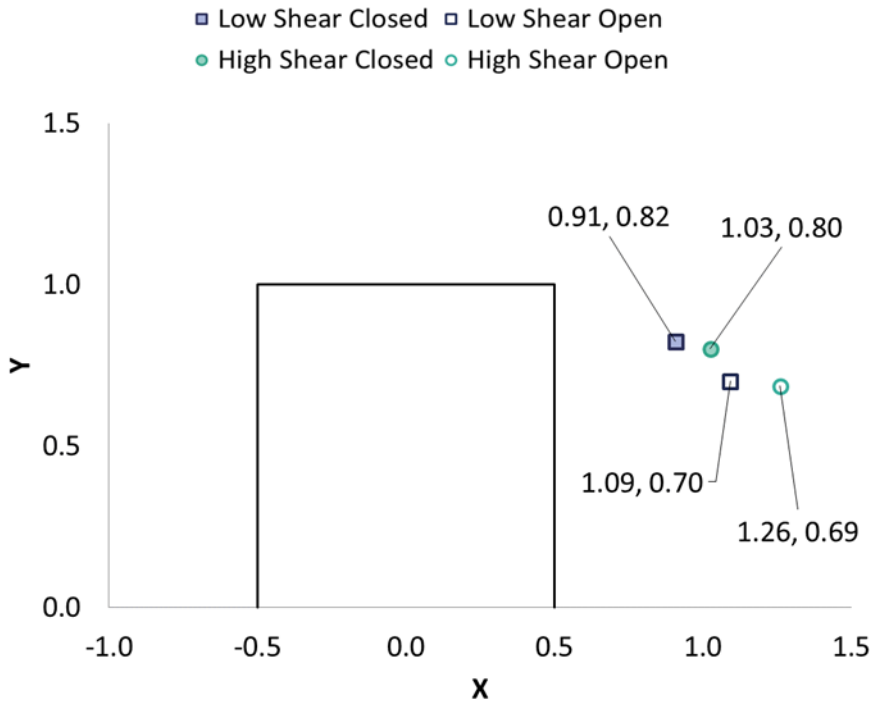

Figure 14. Vortex centres in the wake of the cube for all cases. The flow is from left to right and the coordinates of the vortex centres are also given.

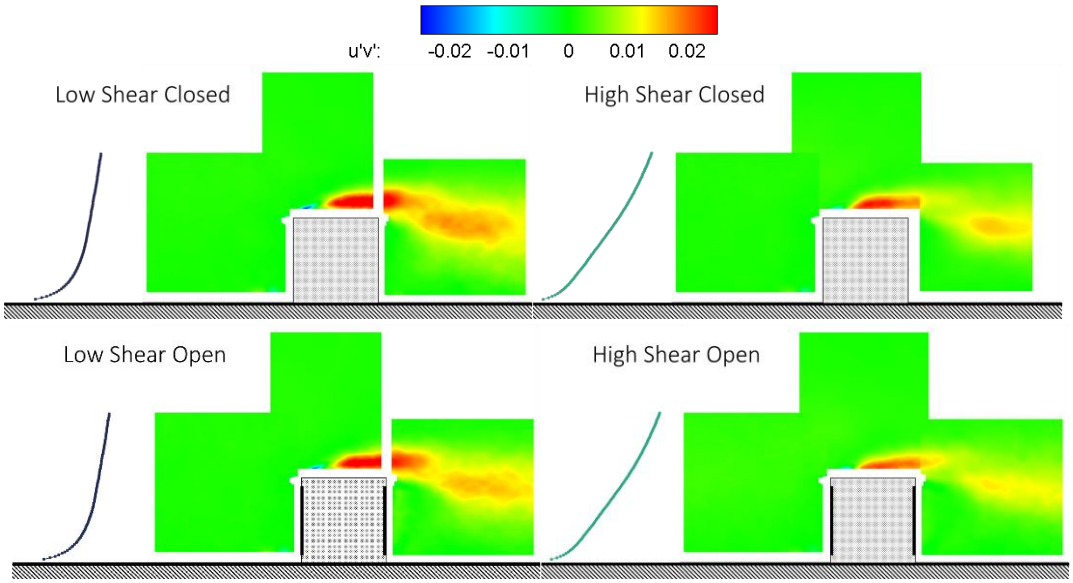

Figure 15. Shear Reynolds stress $\overline{u'v'}$ contours and in-plane flow lines on the planes along the cube centreline (A, B and C) for all cases.

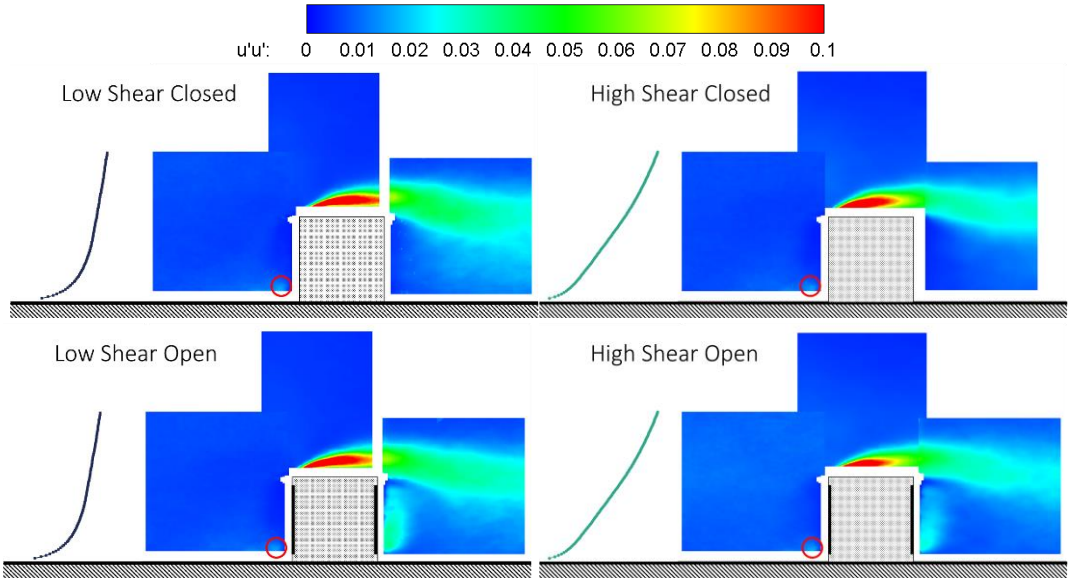

Figure 16. Normal Reynolds stress $\overline{u'u'}$ contours and in-plane flow lines on the planes along the cube centreline (A, B and C) for all cases. Red circles indicate the higher concentration regions caused by the horseshoe vortex instability.

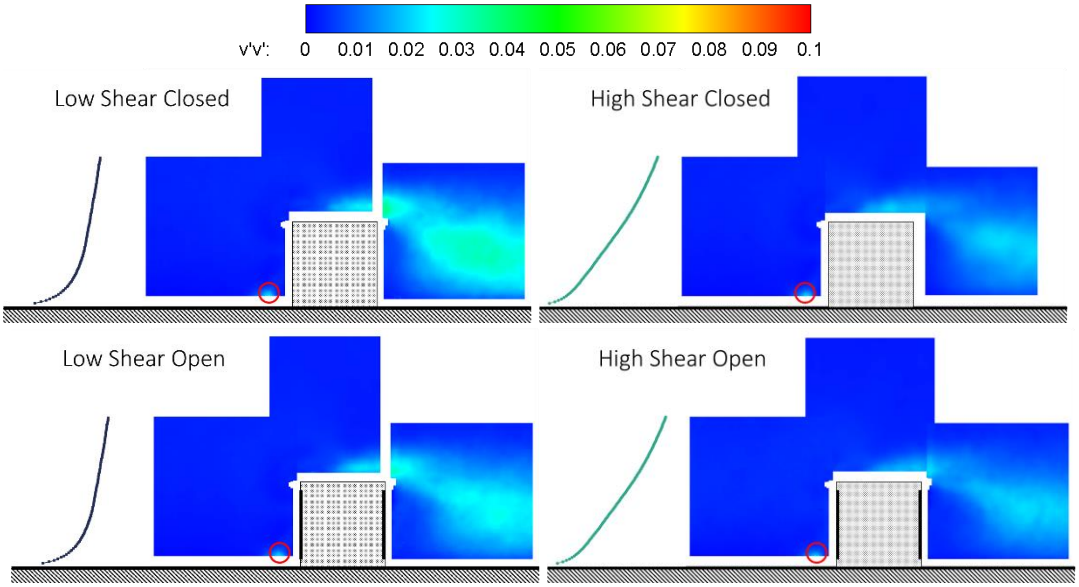

Figure 17. Normal Reynolds stress $\overline{v'v'}$ contours and in-plane flow lines on the planes along the cube centreline (A, B and C) for all cases. Red circles indicate the higher concentration regions caused by the horseshoe vortex instability.

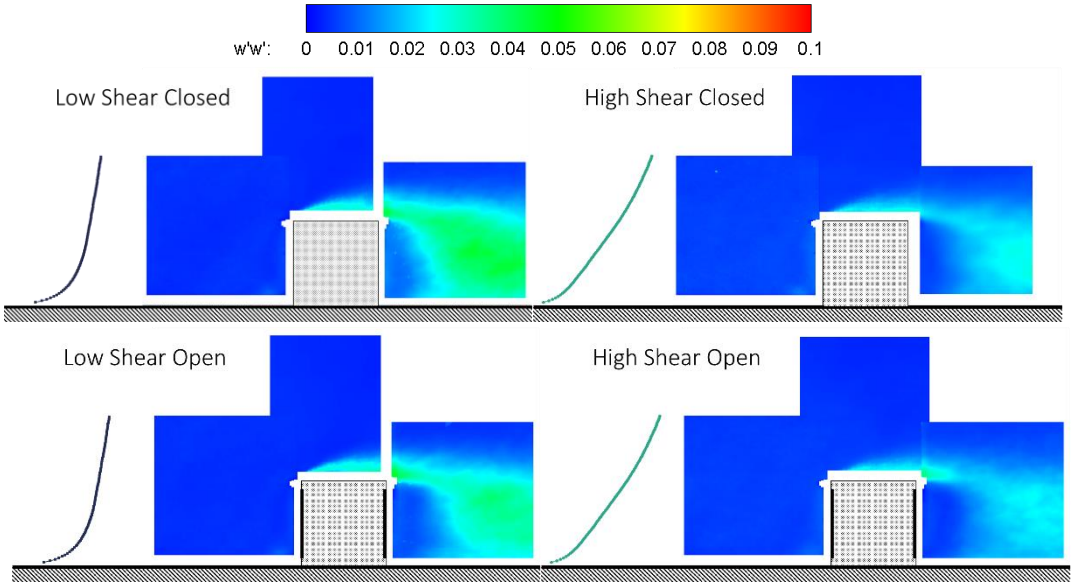

Figure 18. Normal Reynolds stress $\overline{w'w'}$ contours and in-plane flow lines on the planes along the cube centreline (A, B and C) for all cases.

3.3.2 Plane normal to the flow

Figure 19 and Figure 20 show contours of the streamwise vorticity and crossflow velocity on plane D, normal to the flow. Contours of streamwise velocity are shown in Figure 21, while normal Reynolds stress results are given in Figure 22 to Figure 24.

The effect of the openings is to reduce the size and strength of the horseshoe vortex for both inflow cases. Also, the amount of crossflow is reduced in both cases by the presence of the openings. This is understandable as part of the incoming momentum is not rolled up into the horseshoe vortex as it goes through the ventilation openings.

The amount of crossflow is greater for the LS case than the HS case because the higher momentum fluid is diverted by the cube to its sides. Additionally, the streamwise velocity is also increased at the around the cube, as shown in Figure 21.

The normal Reynolds stress ($\overline{v'v'}$) contours shown in Figure 23 also indicate that the high intensity region caused by the horseshoe vortex unsteadiness is greater for LS than HS and for Closed openings than for Open. Further away from the cube (z = -2), the increased values in the HS cases of the normal Reynolds stress are due to the increased turbulence of the incoming flow. Similarly, the region of increased crossflow Reynolds stress (see contours of $\overline{w'w'}$ in Figure 24) is greater for the HS case, as this is affected by the higher turbulence levels of the incoming BL.

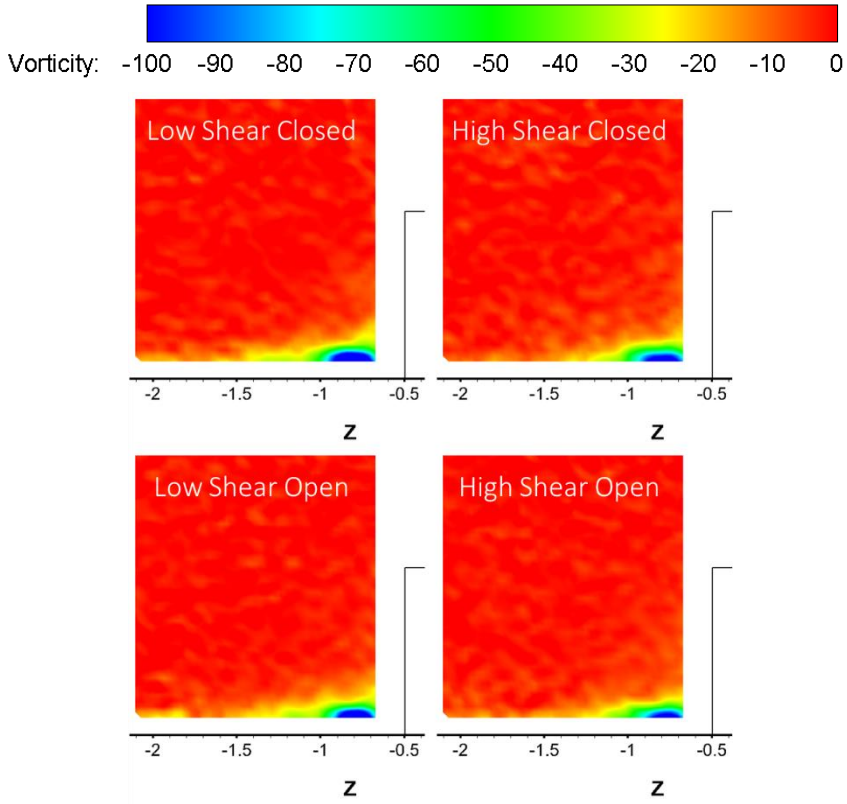

Figure 19. Contours of streamwise vorticity on plane D, normal to the free stream flow, looking downstream.

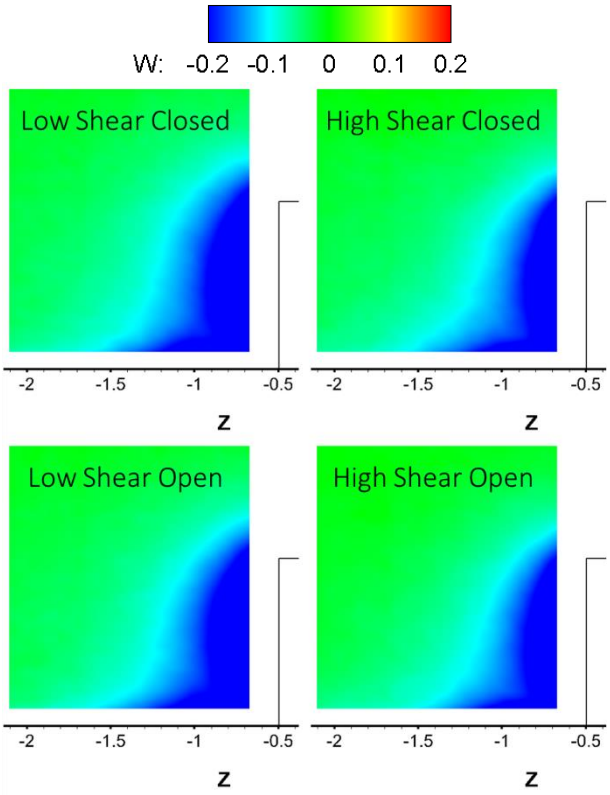

Figure 20. Contours of the crossflow velocity, W, on plane D, normal to the free stream flow, looking downstream.

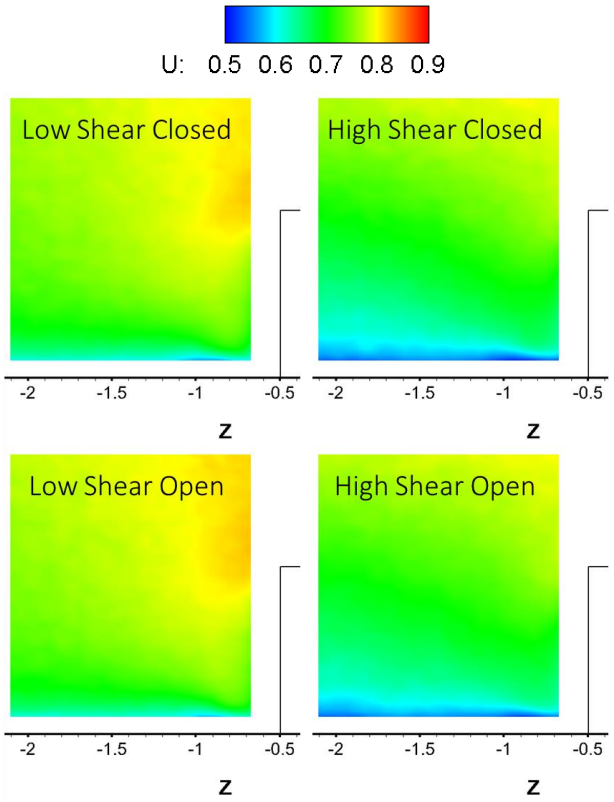

Figure 21. Contours of streamwise velocity U on plane D, normal to the free stream flow, looking downstream.

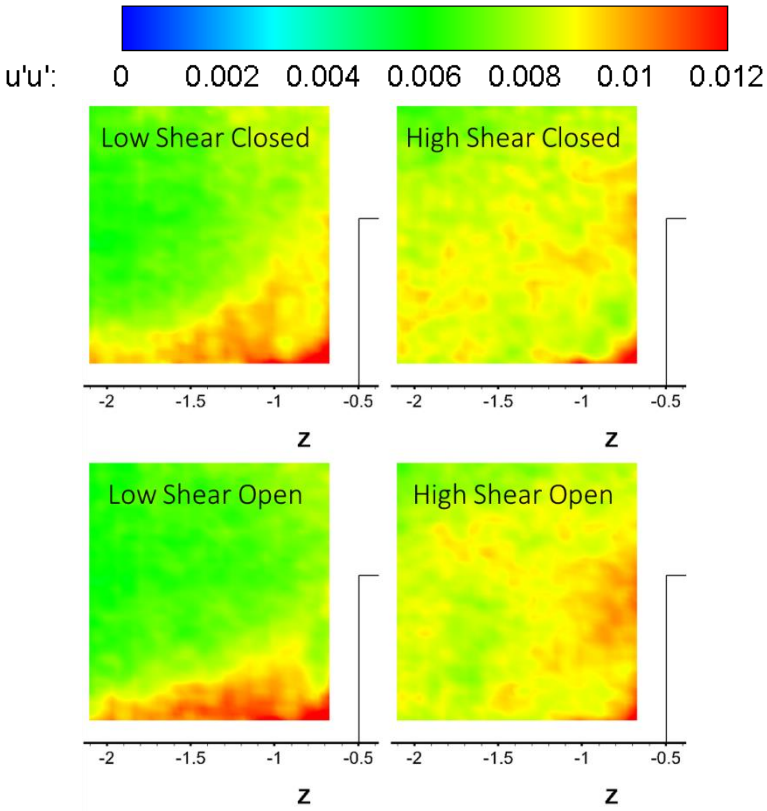

Figure 22. Contours of the $\overline{u'u'}$ normal Re stress on plane D, normal to the free stream flow, looking downstream.

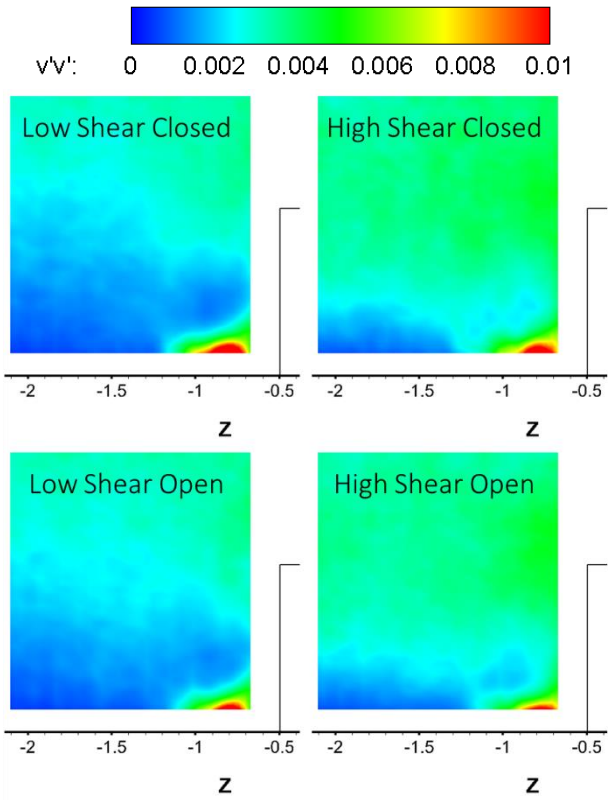

Figure 23. Contours of the $\overline{v'v'}$ normal Re stress on plane D, normal to the free stream flow, looking downstream.

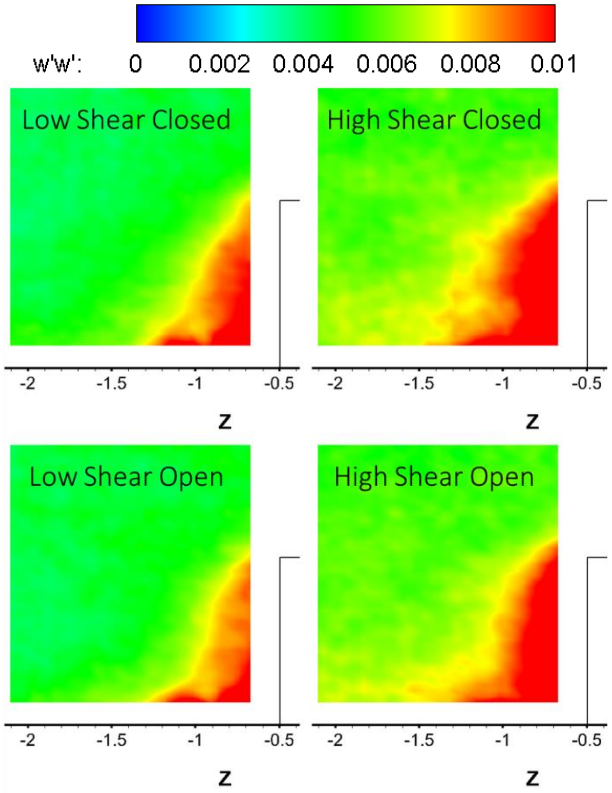

Figure 24. Contours of the $\overline{w'w'}$ normal Re stress on plane D, normal to the free stream flow, looking downstream.

3.4 Cross-ventilation

As shown in Figure 12, the pressure distribution along the vertical opening does vary significantly, which renders the use of the orifice equation and the simplification of the discharge coefficient problematic. In this section, in addition to the orifice equation, the streamwise velocity, U, profile in the vicinity of the apertures will be used to get a more accurate estimate of the ventilation rate. The flow rate, Q, will be calculated using equation (4), where A is the geometric area of the opening. This method is similar to that of Karava et al. [11], with the relative distance of the profile from the cube opening being closer in the present case.

Figure 20 shows streamwise velocity profiles upstream and downstream of the cube for all cases at a distance of approximately 1cm from the cube surface. The cube and its openings are also shown graphically to facilitate understanding. The upstream profiles reveal that in the Open cases the velocity is significantly higher than in the Closed cases with the same inflow. The HS profiles are always slower than the LS cases, as expected.

Downstream of the building model, what defines the velocity profile is the state of the apertures. Both the Open and the Closed cases collapse between them, regardless of the upstream condition. It is interesting to note that negative velocity values are observed at the lower end of the leeward profile for the Open cases.

In the present case it is not justifiable to simply use equation (4), as this would lead to obviously erroneous results (see Figure 25). For example, if the leeward profiles are used, then the flow rate would be the same for both the LS and the HS cases. On the other hand, if the upstream profiles are used, then a different ventilation rate would be obtained for each case, but these would be definitely overestimated, as it is not all the flow that passes through the building. The reason is that the velocity profiles, despite being really close to the cube (0.09h), are affected by the flow around the cube and do not only correspond to the inflow or outflow from the opening.

An estimate of the flow rate, however, can be obtained if the difference between the Open and the Closed upstream velocity profiles are considered, according to equation (5). The underlining assumption is that the increase in velocity in the Open case profile is due to the flow that passes through the cube. The results are given in Table 4, where it can be seen that the LS profile leads to 3% higher ventilation rates. This is due to the fact that cross-ventilation depends on the inflow momentum and the LS profile has greater momentum throughout the opening height.

$$Q = U * A \tag{4}$$

$$U = U_{Open} - U_{Closed} \tag{5}$$

Using a discharge coefficient value of C_D = 0.61 [1] and the pressure data from Figure 12, the flow rate through the openings can be calculated according to equation (6)

$$Q = C_D A_{Eff} U_h \sqrt{Cp_W - Cp_L} \quad (6)$$

where Cp_W and Cp_L are the mean pressure coefficient values along the openings on the windward and leeward sides, respectively. The effective area is $A_{Eff} = A/\sqrt{2}$, where A is the geometric area of the opening.

As shown in Table 4, the orifice equation overpredicts the mean ventilation rate, compared to the velocity profile estimation, by 13% and 16% for the HS and LS cases, respectively. Additionally, the increase in flow rate due to the change in the upstream condition (from HS to LS) is also overpredicted at 6%, compared to the 3% estimation using the velocity profiles.

Table 4. Estimated flow rate values for the Open cases, using the velocity and the orifice equation method. The increase in flow rate between the Low Shear and the High Shear cases is also given, as predicted by the two methods.

Case	Mean Flow Rate Q [m³/s]		Normalized Mean Flow Rate $Q/(U_h A)$		Delta	
	Velocity	**Orifice**	**Velocity**	**Orifice**	**Velocity**	**Orifice**
High Shear	0.00062	0.00070	0.357	0.404	-	
Low Shear	0.00070	0.00081	0.368	0.428	+3%	+6%

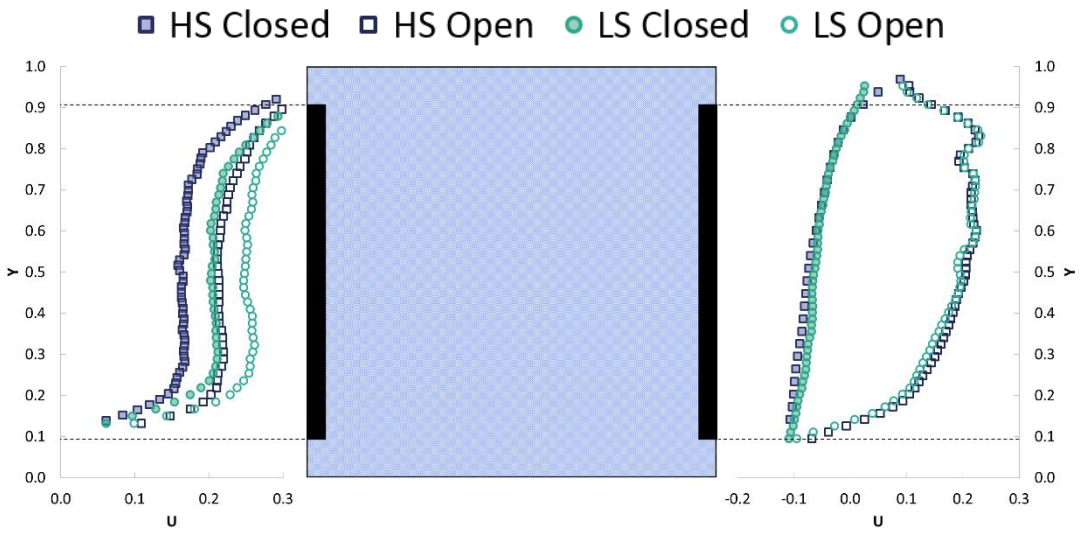

Figure 25. Streamwise velocity profiles upstream and downstream of the cube at a distance of 1cm from the cube surface. Data for the High Shear (HS) and Low Shear (LS) cases with and without openings are shown. The cube and its openings are also shown graphically.

4 Discussion

The present experimental campaign was designed with both the physical problem and its numerical simulation in mind. Pressure and velocity measurements were performed under clearly defined and easy to reproduce conditions. The comparison with published benchmark results gives confidence in the implementation of the experiment. The turbulence content of the simulated BL profiles is also sufficient for this study.

The main technical challenge during the tests was to minimize reflections off the cube surface that would not allow trustworthy Stereo PIV measurements near the model. A minimum distance of 1cm for the nearest velocity vector was achieved, a result as good as other relevant 2D PIV experiments. It is noted that compared to the latter tests, the Stereo PIV set up is more challenging because the two cameras are inclined with respect to the measurement plane.

Both pressure and velocity measurements show that the effect of the upstream BL is important, leading to significant alterations of the flow structure above and in the wake of the cube. The HS inflow leads to smaller recirculation above the cube model and to the formation of a saddle point in the wake, regardless of the apertures' state (open or closed).

A plausible explanation for the differences in the flow structure is the following. In the case of LS inflow, the amount of momentum that needs to be diverted above and to the sides of the building model is larger than in the case of the HS profile. This is because the LS profile is fuller than the HS one closer to the ground (i.e. higher velocities at heights lower than the cube height, see also Figure 6). As a result, the upwash will be stronger in the LS case and consequently the recirculation region above the cube will be larger, as observed by both Stereo PIV and pressure measurements. This thinking also explains the observed differences for the planes normal to the flow.

The difference in the recirculation region leads to the notable differences in the wake region, where in the HS cases a saddle point appears regardless of the openings state. In both Open cases the flow is clearly exiting the vertical cube openings and the outflow joins the vortex in the wake of the cube. The saddle point in the Open HS case is higher and more upstream compared to the Closed case, as the flow is affected by the through-flow from the cube slot. Overall, the effect of the openings is obvious and significant in the wake, but it is weaker than that of the approaching BL upstream and above the cube, in agreement with the pressure data.

The velocity turbulence data reveal that the flow above and in the wake of the cube is more unsteady for the LS cases, with stronger shear layer flapping. The openings, on the other hand, appear to have a stabilizing effect as a well-directed outflow from the slot reduces fluctuations for both upstream cases. At the same time, because of the flow through the openings, the upstream horseshoe vortex moves downstream closer to the cube surface. This effect of the openings is even more noteworthy given their small size (4.5% of the face area).

Orifice equation predictions are compared to ventilation rate estimation based on the velocity measurements near the apertures. The results show that, for the vertical apertures examined in the present report, the orifice equation can provide a prediction within 16% for the ventilation rate. With regard to the effect of the upstream condition, however, the predicted effect is double the one calculated from the measured velocity profiles. It is noted at this point that the present case is particularly challenging for the orifice approximation not only because of the momentum effect, which is not taken into account, but also because of the pressure variation along the cube vertical openings.

5 Conclusions

The present study is an experimental investigation of the atmospheric BL flow past a cubic building model with relatively small (4.5% porosity) vertical openings. The upstream flow

was measured using hot wire anemometry and two different atmospheric BL conditions were simulated. Pressure measurements were taken on the cube surface and velocity measurements around the cube were performed using Stereo PIV. The pressure data compare very well against relevant data from the literature. To the authors' knowledge this is the first time the flow around a cube with vertical openings has been measured using Stereo PIV. The aim of the study was to provide new information regarding the flow past a building model with openings and to generate a data set that may be used for validation purposes. All data are freely available for validation purposes [44].

The effect of the upstream condition (High Shear or Low shear) is significant on the flow around the cube. LS inflow leads to larger recirculation region on the cube roof and higher pressure values on the front face. In the HS case the flow topology in the wake changes and a saddle point appears on the in-plane stream lines. In all cases the centre of the arch-type vortex is evident. The vortex centre moves further downstream and lower for open apertures and if the upstream BL is LS compared to HS. In the Open cases and despite the relatively small size of the apertures, a clearly defined outflow region is observed downstream of the vertical opening. The outflow from the openings is entrained in the arch-type vortex in both cases. The Reynolds stress contours reveal region of intense flow variation and, in general, the flow in the LS case appears to vary more than in the HS case, especially in the wake.

The ventilation rate is estimated using two methods, the orifice equation and the measured velocity profiles near the openings. The orifice equation overpredicts ventilation by 16% or less and overpredicts the effect of the upstream condition by 100%.

6 Acknowledgements

This investigation was supported by the Chinese Academy of Sciences Fellowships for Young International Scientists. Grant Nr 7-160103.

References

[1] Etheridge, D. W. and Sandberg, M. 1996 *Building ventilation: theory and measurement*: John Wiley & Sons Chichester, UK

[2] Finnegan, M.Pickering, C. and Burge, P. 1984 "The sick building syndrome: prevalence studies" *Br Med J (Clin Res Ed)* Vol 289 No 6458 1984 pp 1573-1575

[3] Tzempelikos, A.Athienitis, A. K. and Karava, P. 2007 "Simulation of façade and envelope design options for a new institutional building" *Solar Energy* Vol 81 No 9 2007 pp 1088-1103

[4] Linden, P. F. 1999 "The fluid mechanics of natural ventilation" *Annual Review of Fluid Mechanics* Vol 31 No 1 1999 pp 201-238

[5] Van Hooff, T. and Blocken, B. 2010 "Coupled urban wind flow and indoor natural ventilation modelling on a high-resolution grid: a case study for the Amsterdam ArenA stadium" *Environmental Modelling & Software* Vol 25 No 1 2010 pp 51-65

[6] Etheridge, D. 2011 *Natural ventilation of buildings: theory, measurement and design*: John Wiley & Sons

[7] Ohba, M. and Lun, I. 2010 "Overview of natural cross-ventilation studies and the latest simulation design tools used in building ventilation-related research" *Advances in Building Energy Research* Vol 4 No 1 2010 pp 127-166

[8] Awbi, H. B. 2003 *Ventilation of buildings*: Taylor & Francis

[9] Chen, Q. 2009 "Ventilation performance prediction for buildings: A method overview and recent applications" *Building and Environment* Vol 44 No 4 2009 pp 848-858 doi: http://dx.doi.org/10.1016/j.buildenv.2008.05.025
[10] Kang, J.-H. and Lee, S.-J. 2008 "Improvement of natural ventilation in a large factory building using a louver ventilator" *Building and Environment* Vol 43 No 12 2008 pp 2132-2141
[11] Karava, P.Stathopoulos, T. and Athienitis, A. 2011 "Airflow assessment in cross-ventilated buildings with operable façade elements" *Building and Environment* Vol 46 No 1 2011 pp 266-279
[12] Murakami, S. 1991 "Wind tunnel test on velocity-pressure field of cross-ventilation with open windows" *ASHRAE Transactions* Vol 97 1991 pp 525-538
[13] Kato, S.Murakami, S.Mochida, A.Akabayashi, S.-i. and Tominaga, Y. 1992 "Velocity-pressure field of cross ventilation with open windows analyzed by wind tunnel and numerical simulation" *Journal of Wind Engineering and Industrial Aerodynamics* Vol 44 No 1 1992 pp 2575-2586
[14] Tominaga, Y. and Blocken, B. 2016 "Wind tunnel analysis of flow and dispersion in cross-ventilated isolated buildings: Impact of opening positions" *Journal of Wind Engineering and Industrial Aerodynamics* Vol 155 2016 pp 74-88
[15] Murakami, S. 1990 "Numerical simulation of turbulent flowfield around cubic model current status and applications of k−ϵ model and LES" *Journal of Wind Engineering and Industrial Aerodynamics* Vol 33 No 1 1990 pp 139-152 doi: https://doi.org/10.1016/0167-6105(90)90030-G
[16] Etheridge, D. 2015 "A perspective on fifty years of natural ventilation research" *Building and Environment* Vol 91 2015 pp 51-60
[17] Meroney, R. and Yamada, T. 1972 "Numerical and physical simulation of a stratified airflow over a series of heated islands " *Proceedings of Summer Simulation Conference*.
[18] van Hooff, T.Blocken, B. and Tominaga, Y. 2017 "On the accuracy of CFD simulations of cross-ventilation flows for a generic isolated building: comparison of RANS, LES and experiments" *Building and Environment* Vol 114 2017 pp 148-165
[19] van Hooff, T. and Blocken, B. 2013 "CFD evaluation of natural ventilation of indoor environments by the concentration decay method: CO 2 gas dispersion from a semi-enclosed stadium" *Building and Environment* Vol 61 2013 pp 1-17
[20] Perén, J. I.van Hooff, T.Leite, B. C. C. and Blocken, B. 2015 "CFD analysis of cross-ventilation of a generic isolated building with asymmetric opening positions: Impact of roof angle and opening location" *Building and Environment* Vol 85 No 0 2015 pp 263-276 doi: http://dx.doi.org/10.1016/j.buildenv.2014.12.007
[21] Jiang, Y.Alexander, D.Jenkins, H.Arthur, R. and Chen, Q. 2003 "Natural ventilation in buildings: measurement in a wind tunnel and numerical simulation with large-eddy simulation" *Journal of Wind Engineering and Industrial Aerodynamics* Vol 91 No 3 2003 pp 331-353
[22] Tong, Z.Chen, Y. and Malkawi, A. 2016 "Defining the Influence Region in neighborhood-scale CFD simulations for natural ventilation design" *Applied Energy* Vol 182 2016 pp 625-633 doi: https://doi.org/10.1016/j.apenergy.2016.08.098
[23] Livermore, S. R. and Woods, A. W. 2007 "Natural ventilation of a building with heating at multiple levels" *Building and Environment* Vol 42 No 3 2007 pp 1417-1430
[24] Andersen, K. T. 1996 "Inlet and ouflet coefficients. A theoretical analysis " *5th International Conference on Air Distribution in Rooms ROOMVENT'96*.
[25] Costola, D.Blocken, B. and Hensen, J. 2009 "Overview of pressure coefficient data in building energy simulation and airflow network programs" *Building and Environment* Vol 44 No 10 2009 pp 2027-2036

[26] Chiu, Y.-H. and Etheridge, D. 2004 "Experimental technique to determine unsteady flow in natural ventilation stacks at model scale" *Journal of Wind Engineering and Industrial Aerodynamics* Vol 92 No 3-4 2004 pp 291-313
[27] Schatzmann, M.Rafailidis, S. and Pavageau, M. 1997 "Some remarks on the validation of small-scale dispersion models with field and laboratory data" *Journal of Wind Engineering and Industrial Aerodynamics* Vol 67-68 1997 pp 885-893 doi: https://doi.org/10.1016/S0167-6105(97)00126-8
[28] Tominaga, Y.Mochida, A.Yoshie, R.Kataoka, H.Nozu, T.Yoshikawa, M. and Shirasawa, T. 2008 "AIJ guidelines for practical applications of CFD to pedestrian wind environment around buildings" *Journal of Wind Engineering and Industrial Aerodynamics* Vol 96 No 10 2008 pp 1749-1761 doi: https://doi.org/10.1016/j.jweia.2008.02.058
[29] Yoshie, R.Mochida, A.Tominaga, Y.Kataoka, H.Harimoto, K.Nozu, T. and Shirasawa, T. 2007 "Cooperative project for CFD prediction of pedestrian wind environment in the Architectural Institute of Japan" *Journal of Wind Engineering and Industrial Aerodynamics* Vol 95 No 9 2007 pp 1551-1578 doi: https://doi.org/10.1016/j.jweia.2007.02.023
[30] Tamura, T.Nozawa, K. and Kondo, K. 2008 "AIJ guide for numerical prediction of wind loads on buildings" *Journal of Wind Engineering and Industrial Aerodynamics* Vol 96 No 10 2008 pp 1974-1984
[31] Castro, I. P. and Robins, A. G. 1977 "The flow around a surface-mounted cube in uniform and turbulent streams" *Journal of Fluid Mechanics* Vol 79 No 2 1977 pp 307-335 doi: 10.1017/s0022112077000172
[32] Tieleman, H. W.Ge, Z.Hajj, M. R. and Reinhold, T. A. 2003 "Pressures on a surface-mounted rectangular prism under varying incident turbulence" *Journal of Wind Engineering and Industrial Aerodynamics* Vol 91 No 9 2003 pp 1095-1115
[33] Hearst, R. J.Gomit, G. and Ganapathisubramani, B. 2016 "Effect of turbulence on the wake of a wall-mounted cube" *Journal of Fluid Mechanics* Vol 804 2016 pp 513-530
[34] Blocken, B. 2014 "50 years of Computational Wind Engineering: Past, present and future" *Journal of Wind Engineering and Industrial Aerodynamics* Vol 129 No 0 2014 pp 69-102 doi: http://dx.doi.org/10.1016/j.jweia.2014.03.008
[35] Cao, X.Liu, J. and Jiang, N. 2014 "An Overview of the Applications of Particle Image Velocimetry for Indoor Airflow Field Measurement" *Proceedings of the 8th International Symposium on Heating, Ventilation and Air Conditioning: Volume 3: Building Simulation and Information Management* Springer Berlin Heidelberg Berlin, Heidelberg pp 223-231
[36] Chu, C. R.Chiu, Y.-H.Chen, Y.-J.Wang, Y.-W. and Chou, C.-P. 2009 "Turbulence effects on the discharge coefficient and mean flow rate of wind-driven cross-ventilation" *Building and Environment* Vol 44 No 10 2009 pp 2064-2072
[37] Sandberg, M. 2004 "An alternative view on the theory of cross-ventilation" *International journal of ventilation* Vol 2 No 4 2004 pp 409-418
[38] Vickery, B.RE, B. and CA, K. 1987 "External wind pressure distributions and induced internal ventilation flow in low-rise industrial and domestic structures" *ASHRAE Transactions* Vol 93 1987 pp 2198-2206
[39] Larsen, T. S. and Heiselberg, P. 2008 "Single-sided natural ventilation driven by wind pressure and temperature difference" *Energy and Buildings* Vol 40 No 6 2008 pp 1031-1040
[40] Larsen, T. S. 2006 "Natural ventilation driven by wind and temperature difference " *Faculty of Engineering and Science* PhD Thesis, Aalborg University
[41] Skote, M.Sandberg, M.Westerberg, U.Claesson, L. and Johansson, A. V. 2005 "Numerical and experimental studies of wind environment in an urban morphology"

Atmospheric Environment Vol 39 No 33 2005 pp 6147-6158 doi: https://doi.org/10.1016/j.atmosenv.2005.06.052

[42] Blocken, B. and Carmeliet, J. 2004 "A review of wind-driven rain research in building science" *Journal of Wind Engineering and Industrial Aerodynamics* Vol 92 No 13 2004 pp 1079-1130 doi: https://doi.org/10.1016/j.jweia.2004.06.003

[43] Hayati, A.Mattsson, M. and Sandberg, M. 2018 "A wind tunnel study of wind-driven airing through open doors" *International journal of ventilation* 2018 pp 1-23

[44] "LIET Research - ABL Experiments" Date accessed: 30/04/2018 http://www.liet.ntua.gr/stpivrequest.html

[45] Manolesos, M. and Voutsinas, S. G. 2015 "Experimental investigation of the flow past passive vortex generators on an airfoil experiencing three-dimensional separation" *Journal of Wind Engineering and Industrial Aerodynamics* Vol 142 2015 pp 130-148

[46] Manolesos, M. and Voutsinas, S. G. 2014 "Study of a stall cell using stereo particle image velocimetry" *Physics of Fluids* Vol 26 No 4 2014 p 045101 doi: http://dx.doi.org/10.1063/1.4869726

[47] Foucaut, J. M.Miliat, B.Perenne, N. and Stanislas, M. 2004 "Characterization of different PIV algorithms using the EUROPIV synthetic image generator and real images from a turbulent boundary layer" *Particle Image Velocimetry: Recent Improvements* Springer pp 163-185

[48] Westerweel, J. 2000 "Theoretical analysis of the measurement precision in particle image velocimetry" *Experiments in Fluids* Vol 29 No 1 2000 pp S003-S012

[49] Cowen, E. and Monismith, S. 1997 "A hybrid digital particle tracking velocimetry technique" *Experiments in Fluids* Vol 22 No 3 1997 pp 199-211

[50] Huang, H.Dabiri, D. and Gharib, M. 1997 "On errors of digital particle image velocimetry" *Measurement Science and Technology* Vol 8 No 12 1997 p 1427

[51] Raffel, M.Kompenhans, J. and Willert, C. E. 1998 *Particle image velocimetry: a practical guide* Berlin: Springer

[52] Lim, H. C.Thomas, T. and Castro, I. P. 2009 "Flow around a cube in a turbulent boundary layer: LES and experiment" *Journal of Wind Engineering and Industrial Aerodynamics* Vol 97 No 2 2009 pp 96-109

[53] Zhou, X.Li, J. and Bouris, D. 2016 "Passive Atmospheric Boundary Layer Simulation in the 3.5m X 2.5m Wind Tunnel" *Acta Energiae Solaris Sinica* No Accepted 2016

[54] Manolesos, M.Gao, Z.Zhou, X.Panos, M. and Bouris, D. 2017 "Experimental study of the flow past a cube with openings embedded in a turbulent boundary layer " *10th International Symposium on Turbulence and Shear Flow Phenomena*.

[55] Irwin, H. 1981 "The design of spires for wind simulation" *Journal of Wind Engineering and Industrial Aerodynamics* Vol 7 No 3 1981 pp 361-366

[56] Lim, H. C.Castro, I. P. and Hoxey, R. P. 2007 "Bluff bodies in deep turbulent boundary layers: Reynolds-number issues" *Journal of Fluid Mechanics* Vol 571 2007 pp 97-118

[57] Cook, N. 1978 "Determination of the model scale factor in wind-tunnel simulations of the adiabatic atmospheric boundary layer" *Journal of Wind Engineering and Industrial Aerodynamics* Vol 2 No 4 1978 pp 311-321

[58] Stathopoulos, T. and Surry, D. 1983 "Scale effects in wind tunnel testing of low buildings" *Journal of Wind Engineering and Industrial Aerodynamics* Vol 13 No 1-3 1983 pp 313-326

[59] Hölscher, N. and Niemann, H.-J. 1998 "Towards quality assurance for wind tunnel tests: A comparative testing program of the Windtechnologische Gesellschaft" *Journal of Wind Engineering and Industrial Aerodynamics* Vol 74 1998 pp 599-608

[60] Martinuzzi, R. and Tropea, C. 1993 "The flow around surface-mounted, prismatic obstacles placed in a fully developed channel flow (Data Bank Contribution)" *Journal of Fluids Engineering* Vol 115 No 1 1993 pp 85-92